# DFT analysis and spectral characteristics of *Celecoxib* a potent COX-2 inhibitor

B. Vijayakumar [a], V. Kannappan [b, *], V. Sathyanarayanamoorthi [c]

[a] *Research and Development Centre, Bharathiar University, Coimbatore 641046, India*
[b] *Department of Chemistry, Presidency College, Chennai 600005, India*
[c] *Department of Physics, PSG College of Arts and Science, Coimbatore 641014, India*

## ARTICLE INFO

## ABSTRACT

Extensive quantum mechanical studies are carried out on *Celecoxib* (CXB), a new generation drug to understand the vibrational and electronic spectral characteristics of the molecule. The vibrational frequencies of CXB are computed by HF and B3LYP methods with 6-311++G (d, p) basis set. The theoretical scaled vibrational frequencies have been assigned and they agreed satisfactorily with experimental FT-IR and Raman frequencies. The theoretical maximum wavelength of absorption of CXB are calculated in water and ethanol by TD-DFT method and these values are compared with experimentally determined $\lambda_{max}$ values. The spectral and Natural bonds orbital (NBO) analysis in conjunction with spectral data established the presence of intra molecular interactions such as mesomeric, hyperconjugative and steric effects in CXB. The electron density at various positions and reactivity descriptors of CXB indicate that the compound functions as a nucleophile and establish that aromatic ring system present in the molecule is the site of drug action. Electronic distribution and HOMO − LUMO energy values of CXB are discussed in terms of intra-molecular interactions. Computed values of Mulliken charges and thermodynamic properties of CXB are reported.

## 1. Introduction

Celecoxib or 4-[5-(4-Methylphenyl)-3-(trifluoromethyl) pyrazol-1-yl] benzene sulfonamide is a selective potent COX-2 inhibitor and it is currently approved by Food and Drug Administration for chemoprevention in familial adenomatous polyposis based on demonstrable inhibition of colon polyp formation. It is also used in cancer therapy [1] and proliferation of HCC cell lines [2]. It may be pointed out that celecoxib was shown to be a gastro-intestinally safe anti-inflammatory. CXB is nitrogen containing hetero cyclic compound and there are several reports that this compound is a well-known drug for anti-inflammatory [3—5] and anti-cancer [6,7]. The poor solubility and slow dissolution rate of CXB are major industrial problems, especially for pharmaceutical scientists involved in drug discovery and drug development. It has been found that amorphous CXB nanoparticles showed dramatic improvement in rate as well as extent of in-vitro drug dissolution and oral bioavailability in beagle dogs. The improvement can be attributed to better wettability, increased saturation solubility and surface area, reduced particle size and decreased diffusion layer thickness. Synthesis, characterization and medicinal applications of CXB and it derivatives have been extensively investigated by several authors [1,2,5]. There is need to carry out quantum mechanical studies on CXB molecule to understand the spectral characteristics of this compound. In the present investigation theoretical investigations on the conformation, vibrational and electronic transitions of CXB. Geometrical parameters are reported for the ground state of CXB. IR frequencies, Raman intensities, UV spectral characteristics and HOMO and LUMO energies of CXB are computed using Gaussian 09W program. The computed results are compared with the experimental spectral data. The redistribution of electron density (ED) in various bonding, anti-bonding orbitals and E(2) energies is calculated by NBO analysis to get an evidence for stability of CXB due to various intra-molecular interactions. HOMO- LUMO analysis has been used to establish charge transfer within the molecule. Mulliken population analysis of CXB is also carried out.

* Corresponding author.
  *E-mail addresses:* venu_kannappan@rediffmail.com, vkannappan48@gmail.com (V. Kannappan).

## 2. Experimental

The drug *celecoxib* with a purity of 99.5% is purchased from Sigma Aldrich chemical suppliers (India). Spectra were recorded for CXB with the sample as received. FT-IR spectrum was recorded in the wavenumber region 400–4000 cm$^{-1}$ on a PERKIN ELMER spectrophotometer equipped with mercury, cadmium and tellurium detector in a KBr pellet technique with a resolution of 1.0 cm$^{-1}$. The FT-Raman spectrum was obtained for the compound in the wavenumber region 50–4000 cm$^{-1}$ on a BRUKER RFS27 spectrophotometer equipped with Raman module accessory operating at 1.5 W power with Nd:YAG laser and the excitation wavelength was 1064 nm. The spectra were recorded in the Regional Sophisticated Centre, Indian Institute of Technology, Chennai-600036, India. UV–vis. spectra were recorded on a Shimadzu UV − 1650 model spectrophotometer with quartz cell of 1 cm optical path length. The base line correction was done with the solvents (benzene, water, ethanol and acetone). The absorption spectra were recorded in the wavelength region of 200–600 nm at a scanning rate of 0.2 nm/s and a slit width of 1 cm.

### 2.1. Computational details

The quantum mechanical computations were performed on CXB by using Gaussian 09 program package [8] at the HF and B3LYP [9,10] levels with 6-311++G (d, p) basis set to obtain geometry optimization. Molecular vibrations and their displacement vectors were obtained using Gauss View interface program [11]. A uniform scaling of 0.9533 was adopted for vibrational frequencies obtained from HF/6-311++G (d, p) and a scaling factor of 0.9615 for B3LYP/6-311++G (d, p) method. The computed Raman activities ($S_i$) were converted to relative Raman intensities ($I_i$) using the equation [1] which was derived from the basic theory of Raman scattering [12,13].

$$I_i = \frac{f(\nu_o - \nu_i)^4 S_i}{\nu_i \left[1 - \exp\left[\frac{-hc\nu_i}{K_b T}\right]\right]} \qquad (1)$$

where, $\nu_o$ is the exciting frequency (in cm$^{-1}$), $\nu_i$ is the vibrational wavenumber of the ith normal mode, h, c, and k are universal constants and $f$ is suitably chosen common scaling factor for all the peak intensities. The electronic transitions, vertical excitation energies, absorbance and oscillator strengths of CXB molecule are calculated with the TD-DFT/6-311++G(d,p) method. The MO calculations such as NBO and HOMO−LUMO are performed on CXB by both HF and DFT methods. These results have also been used to calculate the thermodynamic properties such as heat capacity, entropy and enthalpy. Mulliken charges and molecular properties of CXB (dipole moment, mean polarizability and first static hyperpolarizability) are calculated using on the finite field approach.

## 3. Results and discussion

### 3.1. Geometric parameters of CXB

The numbering of various atoms in CXB molecule is shown in Fig. 1. The optimized structural parameters of CXB are calculated by HF and B3LYP methods with 6-311++G(d,p) basis set and these values are given as supplementary data (Table S−1). The bond lengths and bond angles were determined from geometrical parameters obtained from HF and B3LYP methods. It is found from the data in Table S−1 that the bond lengths obtained by both HF and B3LYP methods is comparable. However, bond lengths obtained by
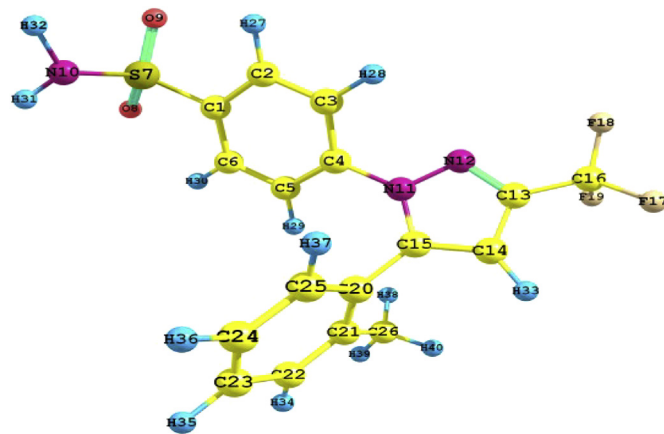


**Fig. 1.** Optimized molecular structure of CXB.

B3LYP method are slightly longer than those calculated by HF method. In the present calculation, amino N−H bond has length of about 1 Å. It is also found that all the six C−C bonds of benzene ring are not of equal length which may be due to −SO$_2$, NH$_2$ group and pyrazole moiety attached to the benzene ring. The effect is also reflected in the bond angles in the benzene ring. It is observed that C2−C1−C6 and C3−C4−C5 bond angles are slightly greater than 120° while C2−C3−C4 and C1−C2−C3 angles are less than 120°. The C−N−C bond angles are slightly larger than the C−C−C or N−C−C bond angles [14]. Gundersen and Rankin have determined the C−N−C (110.7°), C−C−C (109.6°) and N−C−C (110.5°) bond angles in piperidine by electron diffraction technique [15]. In the present study, the bond angles of C4−N11−C15 (129.64°), C14−C13−C16 (127.97°) and N11−C15−C20 (124.78°) by B3LYP/6-311++G(d,p) are greater than 120° indicate the most stable form of CXB molecule. In the pyrazole ring system also C13−C14 bond length is 1.4079 Å and that of C14−C15 bond is 1.3817 Å. This may be attributed to the hetero atom effect of N11 and N12 present as part of the ring system and also due to the adjacent aromatic ring. C13−C14−C15 bond angle is about 105°. However, N12=C13−C14 and N12=C13−C16 bond angles are much larger. Thus, the bond lengths and bond angles in the pyrazole heterocyclic aromatic ring system are influenced by the substituents present in the vicinity of pyrazole ring system. The bond length for C1−S7, N10−H31, S5−N10, S7=O9 and C16−F19 are found to be 1.7970, 1.0150, 1.6937 and 1.4603, 1.3553 Å respectively. The variations in the frequencies or bond lengths are due to the substituents and consequent change in the charge distribution on the carbon atom of the aromatic ring. The substituents may play a very important role on the structural and electronic properties of the molecules. In CXB molecule, the bond length of the group (C−N) is predicted to be 1.4265 Å and it shows good agreement with the experimental data [16] of 1.145 Å.

### 3.2. Analysis of vibrational spectra of CXB

FT-IR and FT-Raman spectra of CXB are recorded in the solid phase, incorporated in KBr pellet. The computed frequency values along with the experimental values are given as supplementary data in Table S−2. It is to be noted that the theoretical frequency calculation is done on the gaseous phase of the molecule using HF and B3LYP methods with 6-311++G (d,p) basis set. CXB molecule consists of 40 atoms and 114 normal vibrational modes are expected as CXB belongs to C1 point group symmetry. The recorded FT-IR and Raman spectra of CXB are depicted in Fig. 2.

The possible modes for amino (NH$_2$) group are symmetric, asymmetric, asymmetric non planar deformation or wagging and
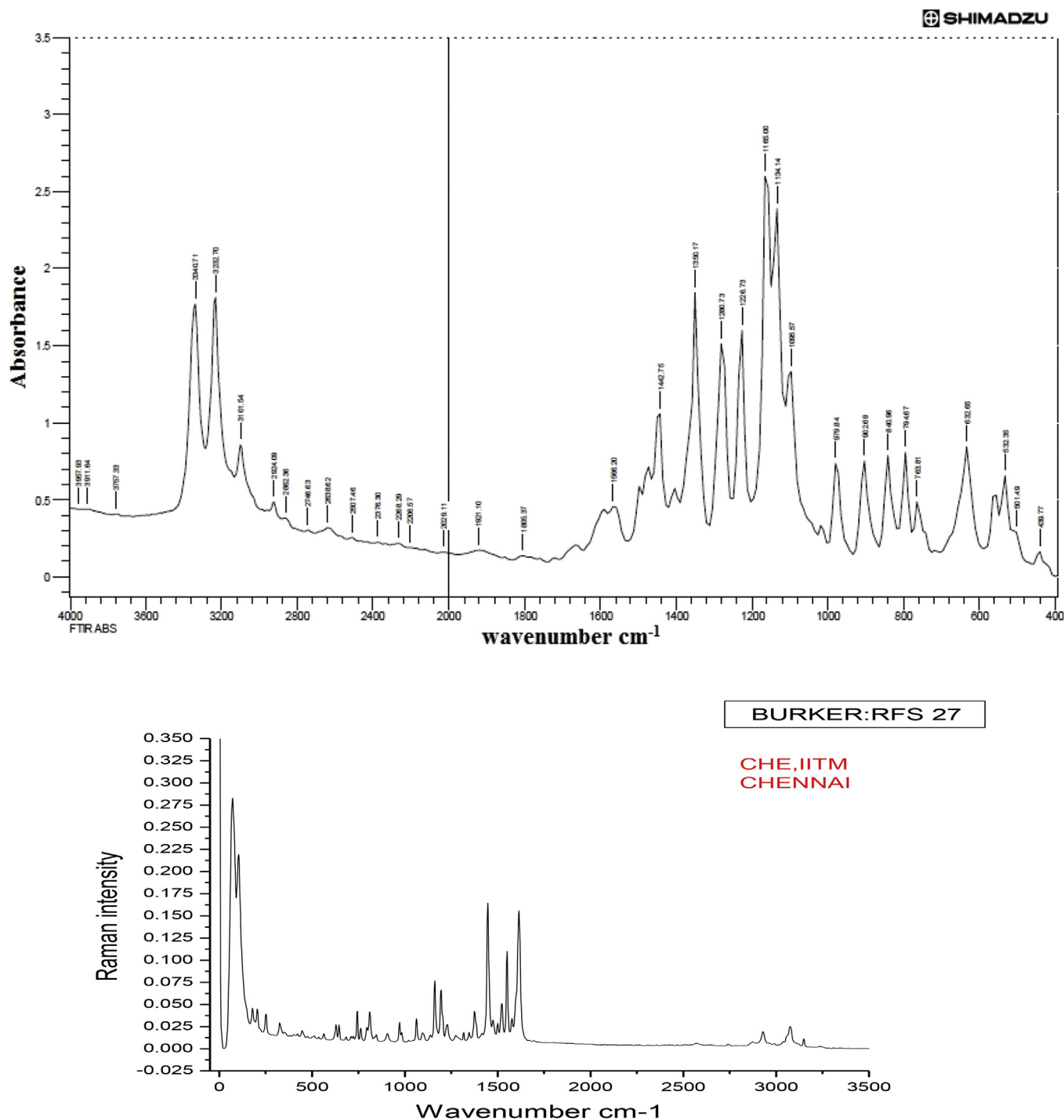
**Fig. 2.** Recorded FT-IR and FT-Raman spectra of CXB.

twisting vibrations. The N–H symmetric stretching vibrations are expected in the region 3500–3300 cm$^{-1}$. The asymmetric –NH$_2$ stretching vibration is in the range [17] 3500–3420 cm$^{-1}$. In the present study, symmetric NH$_2$ stretching is at 3232 cm$^{-1}$ and asymmetric NH$_2$ stretching mode at 3340 cm$^{-1}$ in the recorded spectra of CXB. Computed values for the two modes are 3374, 3485 cm$^{-1}$ (B3LYP) and 3435, 3545 cm$^{-1}$ (HF). There are differences between computed and experimental values and it may be due to intermolecular interactions in the solid state. The NH$_2$ wagging mode is different from the other two stretching modes. The NH$_2$

wagging vibration is similar to the inversion mode of ammonia and it is so strongly anharmonic that it cannot be reproduced by the harmonic treatment [18]. In the present study, the wagging mode of CXB molecule is obtained at 763 cm$^{-1}$ in FT-IR spectrum. It shows better agreement with theoretically value 751 cm$^{-1}$ obtained by B3LYP/6-311++G(d,p) method. The NH$_2$ rocking mode has been reported [19] as 1136 cm$^{-1}$ (IR) and 1133 cm$^{-1}$ (Raman). In the present study, the frequency band obtained at 1064 cm$^{-1}$ in FT-Raman spectrum is assigned to rocking mode. The amino twisting modes are obtained as 492 cm$^{-1}$ and 529 cm$^{-1}$ in HF and as

425 cm$^{-1}$ and 464 cm$^{-1}$in B3LYP method. This band may be too weak to be observed experimentally.

Three fundamental vibrations can be associated with CF$_3$ group. They are two stretching and one in-plane bending modes. In the vibration spectra of CXB, these bands are found over a wide frequency range of 1360–1000 cm$^{-1}$ which may be due to C–F stretching vibrations [20]. The CF$_3$ stretching frequencies were observed at 1142 cm$^{-1}$, 1153 cm$^{-1}$ in HF and 1072 cm$^{-1}$, 1088 cm$^{-1}$ in B3LYP/6-311++G(d,p) methods. We obtained the CF$_3$ in plane bending mode of 1152 cm$^{-1}$ in HF and 1075 cm$^{-1}$ in B3LYP/6-311++G(d,p) methods respectively. The CF$_3$ deformation modes are usually coupled with in-plane bending vibrations.

CXB molecule possesses one methyl group attached to C21 carbon atom. The CH$_3$ group is basically associated with nine fundamentals [21]. In this case, the asymmetric methyl stretching bands are observed at 3075 cm$^{-1}$ in Raman spectra and the value calculated by B3LYP/6-311++G(d,p) agrees with observed frequency. Symmetric and asymmetric deformation vibrations in CH$_3$ group were reported [22] in two regions, namely, 1380–1370 cm$^{-1}$ and 1470–1440 cm$^{-1}$. The two stretching modes are observed at 1486 cm$^{-1}$ and 1501 cm$^{-1}$ in B3LYP/6-311G++(d,p) (modes 90 and 91) and experimental value in FT-Raman is 1501 cm$^{-1}$ the computed value shows good agreement. Methyl rocking mode generally appears as a weak, moderate or sometimes strong band in the region [23] 1050 ± 30 cm$^{-1}$ and 975 ± 45 cm$^{-1}$. This is observed at 1425 cm$^{-1}$ in B3LYP/6-311G++G (d,p). CH$_3$ wagging is observed at 1022 cm$^{-1}$ and computed value is 1424 cm$^{-1}$. The deviation ($\Delta\nu$) of this methyl band is 402 cm$^{-1}$. The methyl twisting and torsion modes are assigned at 134 cm$^{-1}$ and 142 cm$^{-1}$, since CH$_3$ in plane and out of plane bending vibrations are assigned within the characteristic region.

The carbon–carbon stretching modes of the phenyl group are expected in the range from 1650 to 1200 cm$^{-1}$. The actual position of these modes is determined not so much by the nature of the substituent [24]. In the present case, the C–C stretching vibration is found at 1566 cm$^{-1}$ in FTIR and at 1615, 1317 cm$^{-1}$ in FT-Raman spectra. The C–N stretching frequency falls in complicated region of the vibrational spectrum and the mixing of several bands is possible in this region. C–N stretching vibration is assigned in the region 1400–1200 cm$^{-1}$ for aromatic amines [25]. In the present work, the C–N stretching vibration is observed at 1226 cm$^{-1}$ in FTIR and at 1227 cm$^{-1}$ in FT-Raman spectrum. The calculated values are 1292 cm$^{-1}$ and 1246 cm$^{-1}$ in HF/B3LYP respectively.

The heterocyclic aromatic moiety in CXB shows the presence of C–H stretching vibrations in the region 3100–3000 cm$^{-1}$, which is the characteristic region for the prepared recognition of C–H stretching vibration [26]. They are not appreciably affected by the nature of the substituent. In the present study, the calculated wavenumbers of C–H stretching modes are observed at 3310, 3255, 3254, 3240, 3238, 3237, 3236, 3221, 3220 cm$^{-1}$ in HF and 3233, 3173, 3172, 3160, 3159, 3158, 3157, 3143, 3142 cm$^{-1}$ B3LYP methods respectively. The experimental bands are observed at 3101 cm$^{-1}$in FTIR and 3148 cm$^{-1}$in FT-Raman. The C–H in plane bending and C–H out-of-plane bending vibrations are normally found in the range 1000–1300 cm$^{-1}$ and 750–1000 cm$^{-1}$ respectively in the aromatic compounds [27,28]. In agreement with above literature data, the bands observed in FT-IR spectrum at 1350,1134 cm$^{-1}$and in FT-Raman at 1347,1194 cm$^{-1}$ in the present study are due to C–H in plane bending vibrations (Table 2). The IR bands observed at 979,902,840 cm$^{-1}$ and Raman bands observed at 971,907 cm$^{-1}$ are assigned for C–H out-of-plane bending vibration. There is good agreement between theoretically computed C–H vibrational frequencies by B3LYP/6-311++G (d,p) method and experimental wave numbers.

In the vibrational spectra of benzene and its derivatives the ring stretching vibrations are very prominent [29]. According to Varsanyi, the bands are of variable intensity and are observed in the regions [29] 1625–1590 1590–1575, 1540–1470, 1465–1430 and 1380–1280 cm$^{-1}$. The actual positions of these modes are not influenced significantly by the nature of the substituents but by the relative positions of substitution around the ring system [30]. In our present study the wavenumber computed at 1681, 1656,1627, 1622, 1619, 1421,1340 and 690 cm$^{-1}$by B3LYP/6-311++G(d,p) method (mode Nos. 96–100, 84 and 85) are assigned to C–C and C–H stretching vibration for CXB molecule and they show good agreement with recorded FT-IR bands at, 1350 and 1404 cm$^{-1}$ and 1615 and1347 cm$^{-1}$ in FT-Raman spectrum. It may be pointed out that in-plane deformation vibrations are at higher wavenumbers than the out-of-plane vibrations.

### 3.3. Natural bond orbital analysis

The electronic charge transfer and intra molecular interaction within the CXB molecule [31] can be clearly understood by NBO analysis. DFT method predicts satisfactorily the extent of delocalization [32] in organic molecules and the various interactions in CXB molecule from filled orbitals of one atom to vacant orbital of another are investigated by NBO analysis. Larger the E(2) value, the more intensive is the interaction between electron donors and electron acceptors and greater is the tendency of electron donation from donor to acceptor. Consequently, larger is the extent of conjugation in the entire molecular system. Delocalization of electrons present in occupied Lewis type (bonding or non-bonding) orbitals and unoccupied (antibonding) non-Lewis type orbitals shows significant donor–acceptor interaction. The interaction energy is obtained from the second-order perturbation theory [33].

The 17 interactions of the three lone-pairs LP(1), LP(2), LP(3) of fluorine, 16 interactions of the two lone-pairs LP(1), LP(2) of oxygen, 5 interactions involving LP(1) of sulphur and the 9 interactions of the lone-pair LP(1) of nitrogen are assessed using NBO analysis and the results are presented as supplementary data in Tables S–3. Of the five interactions involving LP of S7, three are significant. They are n1 S7 → $\pi^*$ C2–C3, n1 S7 → $\pi^*$ C5–C6 and n1 S7 → $\pi^*$ S7-N10. Thus the LP on sulphur atom interacts with adjacent phenyl carbon atoms, nitrogen and oxygen atoms. It may be noted that there are mutual interaction between O8 and O9 and significant resonance interactions are observed in n3 O8 → $\sigma^*$ S7-O9 and n3 O9 → $\sigma^*$ S7-O8 interactions. It is found that of the three nitrogen atoms only N10 and N12 lone pars are involved in the interaction with neighboring atoms. Of the nine interactions of LP of N10 and N12, two are important. They are n1 N12 → $\sigma^*$ C13–C14 and n1 N12 → $\sigma^*$ C13–C16. It may be pointed out the LP of the three fluorine atoms interact significantly with neighboring carbon and nitrogen atoms. There are 17 interactions involving these three fluorine atoms as donors. They interact mainly with orbitals of N$_{12}$–C$_{13}$, C$_{13}$–C$_{16}$.

### 3.4. Electronic distribution in CXB

The charge distributions calculated by the Mulliken method [34] in the ground state of CXB are presented in Table 1. It can be seen that both HF and B3LYP methods give comparable charge distribution at different positions of CXB molecule. The charge distribution in a molecule influences the vibrational frequencies [35]. CXB molecule is neutral and hence the total charge is zero as it is. The results obtained reveal that the negative charge is delocalized on specific carbon, fluorine, oxygen and nitrogen atoms. In CXB molecule, sulphur, all hydrogen atoms and some of the carbon atoms possess positive charges. Sulphur possesses positive charge due to donor –acceptor interactions between S7 and neighboring oxygen, nitrogen and carbon atoms. Further, these interactions

**Table 1**
Atomic Charges at different positions of CXB.

| Atom | HF/6-311++G(d,p) | | B3LYP/6-311++G(d,p) | |
|------|------------------|------------------|---------------------|------------------|
| | Natural charge | Mulliken charge | Natural charge | Mulliken charge |
| C1 | −0.30 | −0.71 | −0.27 | −0.35 |
| C2 | −0.14 | −0.20 | −0.17 | −0.15 |
| C3 | −0.19 | 0.00 | −0.19 | −0.16 |
| C4 | 0.22 | −0.81 | 0.13 | −0.79 |
| C5 | −0.21 | −0.26 | −0.24 | −0.01 |
| C6 | 0.14 | 0.04 | −0.21 | 0.03 |
| S7 | 2.37 | 0.86 | 2.18 | 0.30 |
| O8 | −1.01 | −0.30 | −0.89 | −0.20 |
| O9 | −1.00 | −0.30 | −0.93 | −0.20 |
| N10 | −1.05 | −0.50 | −1.03 | −0.33 |
| N11 | 0.28 | 0.52 | 0.50 | 0.45 |
| N12 | 0.27 | −0.13 | 0.28 | 0.10 |
| C13 | 0.08 | −0.64 | 0.04 | −0.50 |
| C14 | −0.29 | −0.34 | −0.72 | −0.26 |
| C15 | 0.24 | 0.03 | 0.64 | −0.07 |
| C16 | 1.19 | 0.68 | 1.01 | 0.45 |
| F17 | −0.40 | −0.17 | −0.35 | −0.12 |
| F18 | −0.38 | −0.15 | −0.33 | −0.10 |
| F19 | −0.39 | −0.14 | −0.34 | −0.08 |
| C20 | −0.12 | 0.57 | −0.46 | 0.41 |
| C21 | 0.01 | 0.39 | 0.01 | 0.25 |
| C22 | - 0.19 | −0.28 | 0.23 | −0.16 |
| C23 | - 0.16 | −0.36 | −0.32 | −0.34 |
| C24 | −0.20 | −0.56 | −0.69 | −0.49 |
| C25 | −0.14 | −0.24 | −0.30 | −0.08 |
| C26 | −0.52 | −0.67 | −0.58 | −0.60 |
| H27 | 0.23 | 0.32 | 0.24 | 0.27 |
| H28 | 0.23 | 0.26 | 0.24 | 0.22 |
| H29 | 0.22 | 0.23 | 0.24 | 0.22 |
| H30 | 0.23 | 0.33 | 0.23 | 0.28 |
| H31 | 0.40 | 0.33 | 0.41 | 0.30 |
| H32 | 0.40 | 0.34 | 0.38 | 0.31 |
| H33 | 0.23 | 0.26 | 0.19 | 0.22 |
| H34 | 0.19 | 0.21 | 0.22 | 0.17 |
| H35 | 0.20 | 0.21 | 0.02 | 0.17 |
| H36 | 0.20 | 0.21 | 0.20 | 0.18 |
| H37 | 0.20 | 0.21 | 0.21 | 0.17 |
| H38 | 0.19 | 0.15 | 0.21 | 0.16 |
| H39 | 0.19 | 0.17 | 0.21 | 0.15 |
| H40 | 0.19 | 0.19 | 0.12 | 0.18 |

involve considerable energy of interaction. The carbon atoms of aromatic ring in the molecule have negative charges, except C4. This is also due to interaction between LP of S7 and NBO of aromatic carbon atoms. It may be pointed out that C4 is not involved in these interactions and hence it is positively charged. Very similar values of positive charges are noticed for the hydrogen atoms of CH3 group. However, fluorine atoms of CF3 group are all negatively charged. This is because of mutual LP interaction of one fluorine atom with the orbital of neighboring fluorine atom. It is observed that N10 atom possesses negative charge, while N11 and N12 atoms are positively charged. C14 is negatively charged while C15 is positively charged. In the case of C13 atom, natural charges are positive while Mulliken charges are negative. This suggests that there is resonance involving lone pair of electrons of nitrogen atoms of pyrazole ring. Most of the benzene ring carbon atoms are negatively charged indicating intra-molecular conjugative electron interactions in CXB. For the hydrogen atoms, the differences in calculated charge are relatively smaller. Very smaller value of positive charges is observed for hydrogen atoms connected with carbon atoms of in benzene ring. It may be pointed out that the high values of positive charge are noticed on H27, H30 and H32 which indicate that these hydrogen atoms are involved in hydrogen bonding. The charge increase at the hydrogen atoms taking part in hydrogen bonding is also a clear manifestation of hydrogen bonding. Large values of charge on N10 (negative) and H27−H40

(positive) are due to intramolecular charge transfer. It is observed that the charges computed by HF method are comparable to those obtained by B3LYP method. It is known that CXB is a selective cyclooxygenase-2 (COX-2) inhibitor used for treatment of osteoarthritis and rheumatoid arthritis. It acts by reducing prostaglandin (PG) synthesis through inhibition of COX-2 enzyme. The results suggest that treatment with Celecoxib exacerbates inflammation-associated colonic injury in experimental colitis. The preliminary study showed that the mechanism is related to suppression by the COX-2 inhibitor of the PG derived from COX-2. But further study is needed [36] to establish the chemical interaction between CXB and COX-2. It should be mentioned here that drugs like Celecoxib, rofecoxib and sulindac showed impressive reductions in polyp recurrence but also caused cardiovascular side effects in colorectal clinical prevention trials. Subsequent studies revealed that the adverse cardiovascular effects are mechanism based (i.e., they result from the inhibition of COX-2) and that they are especially relevant to individuals with preexisting risk factors for coronary artery disease [37]. Thus, the investigation carried out so far on the mechanism of CXB − COX-2 interaction does not indicate whether CXB acts as electrophile or nucleophile in its inhibition of COX-2. From the electronic charge distribution obtained in the present study, we can infer that if CXB is an electrophile in the drug action, then the reaction sites may be S7, N11 and N12 which are electron deficient. On the other hand if CXB acts as a nucleophile in the inhibition reaction, then the electron rich aromatic carbon atoms may be the active site of drug action.

### 3.5. Nonlinear optical properties and dipole moment

This part of the study includes dipole moment, molecular polarizability, anisotropy of polarizability and molecular first hyperpolarizability of CXB molecule. To obtain polarizability and hyperpolarizability tensors ($\alpha_{xx}$, $\alpha_{xy}$, $\alpha_{yy}$, $\alpha_{xz}$, $\alpha_{yz}$, $\alpha_{zz}$ and $\beta_{xxx}$, $\beta_{xxy}$, $\beta_{xyy}$, $\beta_{yyy}$, $\beta_{xxz}$, $\beta_{xyz}$, $\beta_{yyz}$, $\beta_{xzz}$, $\beta_{yzz}$, $\beta_{zzz}$), a frequency job output file of Gaussian[8] is employed. The units of $\alpha$ and $\beta$ values of Gaussian output are in atomic units (a.u.) and they are converted into electronic units (esu) using the conversion factors: $\alpha$; 1 a. u. = 0.1482 × $10^{-24}$ esu and $\beta$; 1 a. u. = 8.6393 × $10^{-33}$ esu. The mean polarizability ($\alpha$), anisotropy of polarizability ($\Delta\alpha$) and the average value of the first hyperpolarizability ($\beta$) can be calculated using the equations [2−4].

$$\text{Mean polarisability } \alpha_o = \frac{\alpha_{xx} + \alpha_{yy} + \alpha_{zz}}{3} \quad (2)$$

Anisotropic polarisability

$$(\Delta\alpha) = 2^{-1/2} \left[ (\alpha_{xx} - \alpha_{yy})^2 + (\alpha_{yy} - \alpha_{zz})^2 + (\alpha_{zz} - \alpha_{xx})^2 + 6\alpha_{xz}^2 \right]^{1/2} \quad (3)$$

$$\text{First − order polarisability } \beta_{tot} = \left( \beta_x^2 + \beta_y^2 + \beta_z^2 \right)^{1/2} \quad (4)$$

where,

$$\beta_x = \beta_{xxx} + \beta_{yyy} + \beta_{zzz}$$
$$\beta_y = \beta_{yyy} + \beta_{xxy} + \beta_{yzz}$$
$$\beta_z = \beta_{zzz} + \beta_{xxz} + \beta_{yyz}$$

The parameters described above and electronic dipole moment {($\mu_i$) $i$ = x, y, z)} and total dipole moment $\mu_{tot}$ for CXB molecule are summarized in Table 2. The total dipole moment can be calculated using equation [5].

**Table 2**
Component dipole moment, net dipole moment $\mu_{tot}$ (D), component polarizability, mean polarizability $\alpha_o/10^{-22}$ esu, anisotropy polarizability $\Delta\alpha/10^{-25}$ esu and component and total first hyperpolarizability $\beta_{tot}/10^{-31}$ esu values for CXB.

| Parameters | HF/6-311++G(d,p) | B3LYP/6-311++G(d,p) |
|---|---|---|
| $\mu_x$ | −0.24 | −0.46 |
| $\mu_y$ | 6.99 | 6.57 |
| $\mu_z$ | −2.76 | −2.52 |
| $\mu_{tot}$ | 7.52 | 7.05 |
| $\alpha_{xx}$ | −175.29 | −173.11 |
| $\alpha_{yy}$ | −158.06 | −157.53 |
| $\alpha_{zz}$ | −154.10 | −155.12 |
| $\alpha_{xy}$ | −3.10 | 0.42 |
| $\alpha_{xz}$ | 20.37 | 19.64 |
| $\alpha_{yz}$ | 6.62 | 6.14 |
| $\alpha_o$ | −162.48 | −161.92 |
| $\Delta_\alpha$ | −799.32 | −796.26 |
| $\beta_{xxx}$ | 9.27 | 0.50 |
| $\beta_{xxy}$ | 105.46 | 100.69 |
| $\beta_{xxz}$ | −99.65 | −95.69 |
| $\beta_{yyy}$ | 29.13 | 26.86 |
| $\beta_{yyz}$ | 0.41 | −0.08 |
| $\beta_{xyy}$ | 14.24 | 10.07 |
| $\beta_{xyz}$ | 4.54 | 4.80 |
| $\beta_{xzz}$ | 10.02 | 10.34 |
| $\beta_{zzz}$ | −10.74 | −8.46 |
| $\beta_{yzz}$ | −11.54 | −13.07 |
| $\beta_{tot}$ | 168.39 | 156.25 |

$$\mu_{tot} = \left(\mu_x^2 + \mu_y^2 + \mu_z^2\right)^{1/2} \qquad (5)$$

Generally, molecules with large values of dipole moment, molecular polarizability, and hyperpolarizability exhibit NLO properties. The calculated dipole moment of CXB is 7.5195 D in HF method and 7.0491 D in B3LYP/6-311++G (d, p) method. The high dipole moment of CXB is observed for component $\mu_y$. In this direction, this value is equal to 6.9914 D and 6.5666 D in HF and B3LYP methods respectively. The value of $\mu_x$ is the smallest one as −0.2368 D (HF) and −0.4638 D (B3LYP). The calculated polarizability and anisotropy of the polarizability of the title molecule are almost same in the HF and DFT methods. The magnitude of the first hyperpolarizability $\beta_{tot}$, is one of important key parameters in deciding NLO property of a molecule. The highest value of first hyperpolarizability ($\beta_{tot}$) (168.39 × $10^{-33}$ esu) is obtained in method of HF/6-311++G (d, p) method. It is interesting to note that the first hyperpolarizability of CXB is more than twenty times greater than that of urea, one of the prototypical molecules used in the study of the NLO properties. On the basis of high values of dipole moment and first hyperpolarizability it may be concluded that CXB can possess significant NLO properties. It may be noted that the anisotropy polarizability ($\Delta\alpha$) of CXB molecule is also high as obtained in both the methods and the molecule is expected to exhibit NLO properties.

### 3.6. HOMO−LUMO energy

Organic molecules containing conjugated π electrons are characterized by high hyperpolarizabilities and analyzed by means of vibrational spectroscopy [38,39]. In most cases, the strongest bands in the Raman spectrum are weak in the IR spectrum and vice versa even in absence of inversion symmetry. But the intramolecular charge transfer from the donor to accepter group through conjugated bonds can induce large variation in both the molecular dipole moment and molecular polarizability, making IR and Raman bands relatively strong. The experimental spectroscopic behavior described above is well accounted for by HF calculations in π conjugated systems that predict exceptionally large Raman and Infrared intensities for the same normal modes. It is also observed in CXB molecule common bands are observed in FT-IR and Raman spectra indicating that CXB is not a Centro symmetric molecule. The relative intensities in IR and Raman spectra are comparable resulting from the intra molecular electron transfer through π conjugated frame.

Energies of highest occupy molecular orbital (HOMO) and lowest unoccupied molecular orbital (LUMO) are useful and important parameters in quantum chemistry. The frontier molecular orbitals (FMOs) play important role in the optical and electric properties as well as in UV−visible spectra [40] of organic molecules. HOMO, the outer most orbital containing electrons, has the tendency to give electrons and acts as an electron donor. On the other hand LUMO, the inner most orbital containing is vacant and has the ability to accept electrons [41]. As a result of the interaction between HOMO and LUMO orbital, transition state transition of π−π* type is observed with regard to the molecular orbital theory [42]. Therefore, the energy of the HOMO is directly related to the ionization potential while LUMO energy is directly related to the electron affinity. Energy difference between HOMO and LUMO orbital is referred to as the energy gap and it determines the stability of structure [43]. The HOMO-LUMO energy diagram is given in Fig. 3.

### 3.7. Global and local reactivity descriptors

The energy gap between HOMO and LUMO determines electrical transport properties in inorganic and organic molecules. The global chemical reactivity descriptors of organic molecules such as hardness, chemical potential, softness, electronegativity and electrophilicity index as well as local reactivity can be calculated from HOMO and LUMO energy values [44−48]. Pauling introduced the



**LUMO=0. 6013 eV**

**HOMO=−9.5689 eV**
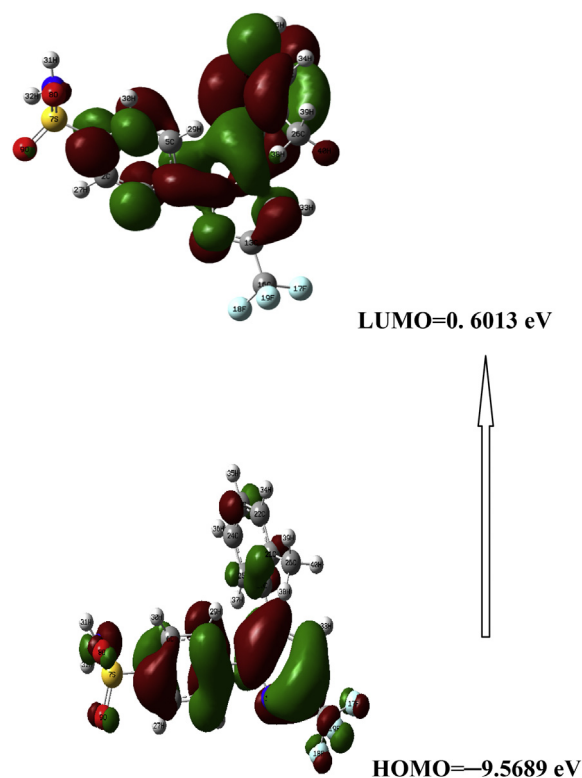
**Fig. 3.** HOMO − LUMO energy diagram of CXB; Energy gap ΔE = 10.1703 eV.

concept of electronegativity as the power of an atom in a molecule to attract electrons towards it. Values of hardness ($\eta$), chemical potential ($\mu$), electronegativity ($\chi$) and softness for CXB are calculated using equations given by earlier workers [44–48]. Softness ($\sigma$) of a molecule that measures the extent of chemical reactivity. It is the reciprocal of hardness. Since CXB is a closed-shell molecules, $\eta$, $\mu$ and $\chi$ are computed from ionization potential and electron affinity using Koopman's theorem (Table 3). The ionization energy and electron affinity were computed from HOMO and LUMO orbital energies. The ionization potential calculated by HF and B3LYP methods for CXB is 10.1703 eV and 5.3734 eV respectively. Generally, a large HOMO–LUMO energy gap means a hard molecule and small HOMO– LUMO gap means a soft molecule. The stability of a molecule and its reactivity can be related to hardness. A molecule with least HOMO–LUMO energy gap (soft molecule) is more reactive. Parr et al. [44] have proposed electrophilicity index ($\omega$) as a measure of energy lowering due to maximal electron flow between donor and acceptor. It is defined by equation [6].

$$\omega = \frac{\mu^2}{2\eta} \tag{6}$$

Using the above equation electrophilicity index is calculated for CXB and it is shown in Table 3. The usefulness of this new reactivity parameter has been recently demonstrated in understanding the toxicity of various pollutants in terms of their reactivity and site selectivity [49–53]. Domingo et al. Proposed that electrophilic index indicates the electrophilic site in organic reactions [54]. A strong and more reactive nucleophile is characterized by a lower value of $\mu$. On the other hand, a good electrophile is characterized by a high value of $\mu$ and $\omega$. The electronegativity and hardness are used extensively are to predict the reactivity and aromatic behavior in organic compounds [55]. In the present computational study, HF method gave higher values of HOMO-LUMO energy gap and chemical hardness than B3LYP method. Similar values of other molecular properties are obtained in both the methods. CXB molecule has very low values of $\mu$, $\omega$ indicating that CXB acts more as a nucleophile than an electrophile. Relatively high values of HOMO-LUMO energy gap and chemical hardness indicate significant aromatic character of CXB. This is probably due to the presence of two benzene rings and one pyrazole ring in CXB molecule. Considering the values of $\mu$, $\omega$ and $\eta$ of CXB, it can be inferred that it acts as a nucleophile in its drug action. The aromatic carbon atoms are rich as evidenced from the electronic distribution in CXB molecule and this may be the active site of drug action.

### 3.8. Analysis of UV–visible spectra

Experimental electronic spectra measured in water and ethanol solutions are presented in Fig. 4. Three bands are expected in the electronic spectra of CBX in the two solvents used in the present investigation (Table 4). These absorptions are due to $\pi$–$\pi^*$ and n-$\pi^*$ transitions. The $\lambda_{max}$ at short wave length is due to $\pi$–$\pi^*$ transition and those at longer wave lengths are due to n-$\pi^*$ transitions. It is to be pointed out that there is bathochromic shift in both the computed and experimental absorptions as we go from less polar solvent to more polar solvent [56]. The observed $\lambda_{max}$ values agree well with the computed values in both the solvents. However, the computed $\lambda_{max}$ values are greater than observed $\lambda_{max}$ values. This may be due to inter molecular hydrogen bond interaction between solvent molecules and CXB molecule. Molecular orbital coefficients analyses based on the optimized geometry indicate that electronic transitions corresponding to above electronic spectra are mainly LUMO and HOMO-LUMO for the title compound. Fig. 3 shows the surfaces of HOMO and LUMO in CXB molecule.

### 3.9. Thermodynamic properties

The standard thermodynamic functions: such as self-consistent field (SCF) energy, zero-point vibrational energies (ZPVE), thermal energies, molar capacities at constant volume, entropy, enthalpy and dipole moment of CXB molecule are calculated at 298 K by HF and B3LYP methods using 6-311++G(d,p) as basis set and these computed values are listed in Table 5. It is found that total energy obtained in HF and B3LYP methods are comparable. With regard to other thermodynamic properties, HF method yielded higher values than those obtained by B3LYP method. The highest value of ZPVE of CXB is 810.39 kJ mol$^{-1}$ obtained in HF/6-311++G (d, p) method. These standard thermodynamic functions for the title molecule were calculated at 298 K using Perl script [57] THERMO. PL. The zero point vibrational energy obtained by HF method is greater than that obtained in B3LYP method. Molar heat capacity at 298 K is high indicating high vibrational contribution. The values of Gibb's free energy, enthalpy and entropy of CXB obtained by HF method are comparable to those obtained by B3LYP method. The thermodynamic functions may give useful information regarding mechanism of drug action on CXB. These values can be used to compute the changes in thermodynamic properties and estimate feasibility of chemical reactions using second law of thermodynamics in thermochemical field [58,59]. It must be remembered that all thermodynamic functions were calculated for CXB in gas phase and suitable solvation correction is to be included when investigation is done in a medium.

### 4. Conclusions

In the present study, we have used the HF and DFT/B3LYP methods to investigate theoretical analysis on the geometries and electronic properties of Celecoxib, a new generation non-steroidal anti-inflammatory drug (NSAID), which acts mainly by the inhibition of COX-2 isoenzyme. The geometry was optimized and bond lengths and bond angles were obtained by HF and DFT methods. It may be pointed out that the bond lengths obtained by both HF and B3LYP methods are comparable and the bond lengths obtained by B3LYP method are slightly longer than those calculated by HF method. The comparison between the calculated vibrational frequencies and the experimental FT-IR and Raman spectra support each other. NBO analysis is used to assess the intra-molecular delocalization in the molecule. It revealed that interaction energy in this molecule is due to electron donation from LP(1)N7 to the BD*(2)C10–C13 which leads to the strongest stabilization of 38.68 kJ/mol. CXB molecule has very low values of $\mu$, $\omega$ indicating that it acts more as a nucleophile than an electrophile. Relatively high values of HOMO-LUMO energy gap and chemical hardness indicate significant aromatic character of CXB. The electronic distribution, in conjunction with electrophilicity index ($\omega$) of CXB

**Table 3**
HOMO, LUMO energy values, chemical hardness ($\eta$), electronegativity ($\chi$), chemical potential ($\mu$), electrophilicity index ($\omega$) and softness ($\sigma$) of CXB in gas phase.

| Parameters | HF/6-311++G (d,p) | B3LYP/6-311++G(d,p) |
|---|---|---|
| $E_{total}$ (kJ/mol$^{-1}$) | $-8.8 \times 10^5$ | $-9.0 \times 10^5$ |
| $E_{HOMO}$ (eV) | $-9.8$ | $-7.4$ |
| $E_{LUMO}$ (eV) | 0.6 | $-2.0$ |
| $\Delta E_{HOMO-LUMO}$ (eV) | 10.2 | 5.4 |
| Chemical hardness ($\eta$) | 5.1 | 2.7 |
| Electronegativity ($\chi$) | 4.5 | 4.7 |
| Chemical potential ($\mu$) (eV) | $-4.5$ | $-4.7$ |
| Electrophilicity index ($\omega$) | 16.6 | 7.1 |
| Softness ($\sigma$) | 0.2 | 0.4 |

(a)



(b)

**Fig. 4.** Experimental UV spectra of CXB in (a) water (b) ethanol.

**Table 4**
Computed electronic spectral data of CXB (wavelength of maximum absorption, $\lambda$ (nm), excitation energies E (eV) and oscillator strengths (f) (a.u)) using TD-DFT/B3LYP/6-311++G (d,p) method along with observed $\lambda_{max}$ values in different solvents.

| Solvent | Obs. $\lambda_{max}$ | $\lambda$ (nm) | $\Delta E$ (eV) | $f$ (a.u.) |
|---------|---------|---------|---------|---------|
| Water | 346.00 | 370.80 | 3.34 | 0.0564 |
|  | 314.00 | 319.79 | 3.87 | 0.0164 |
|  | 250.00 | 300.74 | 4.12 | 0.0070 |
| Ethanol | – | 371.13 | 3.34 | 0.0018 |
|  | 254.00 | 319.39 | 3.88 | 0.0167 |
|  | 206.00 | 301.19 | 4.11 | 0.0062 |

**Table 5**
Computed total energies (a.u.), zero point vibrational energy (kJ mol$^{-1}$), thermal energy (kJ mol$^{-1}$), molar heat capacity (J mol$^{-1}$ K$^{-1}$) ($C_{p,m}^{o}$), standard molar entropy (J K$^{-1}$ mol$^{-1}$) ($S_{m}^{o}$), standard Gibbs free energy (kJ mol$^{-1}$) ($G_{m}^{o}$) and standard enthalpy ($H_{m}^{o}$) (kJ mol$^{-1}$) of CXB by HF and B3LYP methods.

| Parameters | HF/6-311++G(d,p) | B3LYP/6-311++G(d,p) |
|---------|---------|---------|
| SCF energy | −1661.06 | −1668.96 |
| Zero-Point Vibrational Energy | 810.39 | 759.73 |
| Thermal Energy | 862.48 | 815.67 |
| Molar capacity at constant volume | 322.96 | 349.02 |
| Entropy | 606.68 | 652.70 |
| Gibbs free energy | 683.94 | 622.76 |
| Enthalpy | 864.83 | 818.10 |

indicates that the drug functions as a nucleophile and aromatic ring systems present in the molecule are the sites of its function as COX-2 inhibitor. Electronic absorption maxima are computed by TD-DFT method in two different solvents and compared with experimental

$\lambda_{max}$ values. Shift in $\lambda_{max}$ values is observed in different solvents and the trend is discussed in terms of solute-solvent interactions. The standard thermodynamic functions (self-consistent field energy, zero-point vibrational energies (ZPVE), thermal energies, molar capacities at constant volume, entropy, enthalpy and dipole moment of CXB molecule are calculated at 298 K by HF and B3LYP methods using 6-311++G(d,p) as basis set. These parameters can be used to compute the changes in thermodynamic properties and estimate feasibility of chemical reactions using second law of thermodynamics.

## Appendix A. Supplementary data

Supplementary data related to this article can be found at http://dx.doi.org/10.1016/j.molstruc.2016.04.070.

## References

[1] J.M. Bock, S.G. Menon, L.L. Sinclair, N.S. Bedford, P.C. Goswami, F.E. Domann, D.K. Trask, Celecoxib toxicity is cell cycle phase specific, Cancer Res. 67 (2007) 3801–3808.

[2] M.A. Kern, D. Schubert, D. Sahi, M.M. Schöneweifs, I. Moll, A.M. Haugg, H.P. Dienes, P. Schirmacher, P. Breuhahn, Proapoptotic and antiproliferative potential of selective cyclooxygenase-2 inhibitors in human liver tumor cells, Hepatology 36 (2002) 885–894.

[3] N. Bhala, J. Emberson, A. Merhi, S. Abramson, N. Arber, J.A. Baron, C. Bombardier, C. Cannon, M.E. Farkouh, G.A. FitzGerald, P. Goss, H. Halls, E. Hawk, C. Hawkey, C. Hennekens, M. Hochberg, L.E. Holland, P.M. Kearney, L. Laine, A. Lanas, P. Lance, A. Laupacis, J. Oates, C. Patrono, T.J. Schnitzer, S. Solomon, P. Tugwell, K. Wilson, J. Wittes, C. Baigent, Vascular and upper gastrointestinal effects of non-steroidal anti-inflammatory drugs: meta-analyses of individual participant data from randomised trials, Lancet 382 (2013) 769–779.

[4] M. Elliott, E.M. Antman, S. Joel, J.S. Bennett, Alan Daugherty, Curt Furberg, Harold Roberts, K.A. Taubert, Use of nonsteroidal antiinflammatory drugs. An update for clinicians: a scientific statement from the American Heart Association, circulation, Lancet 115 (2007) 1634–1642.

[5] S Guniz Kuçukguzel, Inci Coskun, Sevil Aydın, Goknur Aktay, Sule Gursoy, Ozge Cevik, Ozlem Bingol Ozakpınar, Derya Ozsavcı, Azize Sener, Neerja Kaushik-Basu, Amartya Basu, T. Tanaji, T. Talele, Synthesis and characterization of celecoxib derivatives as possible anti-inflammatory, analgesic, antioxidant, anticancer and anti-HCV agents, Molecules 18 (2013) 3595–3614.

[6] S. Assefnia, S. Dakshanamurthy, J.M. Guidry Auvil, C. Hampel, P.Z. Anastasiadis, B. Kallakury, A. Uren, D.W. Foley, M.L. Brown, L. Shapiro, M. Brenner, D. Haigh, S.W. Byers, Cadherin-11 in poor prognosis malignancies and rheumatoid arthritis: common target, common therapies, Oncotarget 5 (2014) 1458–1474.

[7] A.A. Bekhit, H.M. Ashour, Y.S. Abdel Ghany, Bekhit Ael-D, A. Baraka, Synthesis and biological evaluation of some thiazolyl and thiadiazole derivatives of 1H-pyrazole as anti-inflammatory antimicrobial agents, Eur. J. Med. Chem. 43 (2008) 456–463.

[8] M.J. Frisch, et al., Gaussian 09, Revision B 04, Gaussian Inc., Pittsburg, PA, 2003.

[9] A.D. Becke, Density-functional thermochemistry. III. The role of exact exchange, J. Chem. Phys. 98 (1993) 5648–5652.

[10] C. Lee, W. Yang, R.G. Parr, LYP Gradient-corrected functional, Phys. Rev. B 37 (1993) 5648–5652.

[11] A. Frisch, A.B. Neilson, A.J. Holder, GAUSSVIEW, User Manual, Gaussian Inc., Pittsburgh, CT, 2009.

[12] G. Keresztury, S. Holly, G. Verga Besenyei, A.Y. Wang, J.R. Durig, Vibrational spectra of monothiocarbamates-II. IR and Raman spectra, vibrational assignment, conformational analysis and ab initiocalculations of S-methyl-N,N-dimethylthiocarbamate, Spectrochim, Acta, Part A 49 (1993) 2007–2026.

[13] G. Keresztury, J.M. Chalmers, P.R. Griffiths, Raman Spectroscopy: Theory in Handbook of Vibrational Spectroscopy, Vol. 1, John Wiley & Sons, London, 2002, pp. 71–87.

[14] E. Vayner, D.W. Ball, Ab initio and density functional optimized structures, proton affinities, and heats of formation for aziridine, azetidine, pyrrolidine, and piperidine, J. Mol. Struct. (Theochem) 496 (2000) 175–183.

[15] Grete Gundersen, D.W.H. Rankin, The gas phase molecular structure of piperidine by electron diffraction, Acta Chem. Scand. Part A 37 (1983) 865–874.

[16] P. Pulay, G. Fogarasi, G. Pongor, J.E. Boggs, A. Vargha, Combination of theoretical ab initio and experimental information to obtain reliable harmonic force constants. Scaled quantum mechanical (QM) force fields for glyoxal, acrolein, butadiene, formaldehyde, and ethylene, J. Am. Chem. Soc. 105 (1983) 7037–7047.

[17] Maitland Jones Jr., Steven A.Fleming, Organic Chemistry, IV, W.W. Norton & Company, New York, 2010, pp. 710–712.

[18] P.M. Wojciechawski, W. Zierkiewicz, D. Michalska, P. Hobza, J. Chem. Phys. 118 (2003) 1070–1090.

[19] A. Sumayya, C.Y. Panicker, H.T. Varghese, B. Harikumar, Vibrational spectroscopic studies and ab initio calculations of L-glutamic acid 5-amide, Rasayan J. Chem. 1 (2008) 548–555.

[20] S. Gunasekaran, S. Seshadri, S. Muthu, Vibrational spectra and normal coordinate analysis of flucytosine, Indian J. Pure Appl. Phys. 44 (2006) 581–586.

[21] P.S. Kalsi, Spectroscopy of organic compounds, VI, New Age International (P) Limited, New Delhi, 2005.

[22] D.L. Vien, N.B. Colthup, W.G. Fateley, J.G. Grasselli, Handbook of Infrared and Raman Characteristic Frequencies of Organic Molecules, Academic Press, Boston, 1991.

[23] N.P.G. Roeges, A Guide to the Complete Interpretation of Infrared Spectra of Organic Structures, Wiley, New York, 1994.

[24] L.J. Bellamy, The Infrared Spectra of Complex Molecule, III, Wiley, New York, 1975.

[25] M. Silverstein, G.C. Basseler, C. Morill, Spectrometric Identification of Organic Compounds, Wiley, New York, 1981.

[26] V.K. Rastogi, M.A. Palafox, R.P. Tanwar, L. Mittal, 3,5-Difluorobenzonitrile: ab initio calculations, FTIR and Raman spectra, Spectrochim. Acta Part A 58 (2002) 1987–2004.

[27] V. Balachandran, G. Santhi, V. Karpagam, Spectroscopic (FT-IR and FT-Raman) studies, NBO, HOMO–LUMO, NMR analyses and thermodynamics functions of 5-bromo-2-methoxybenzaldehyde, Spectrochim. Acta Part A 106 (2013) 262–274.

[28] A. Altun, K. Golcuk, M. Kumru, Theoretical and experimental studies of vibrational spectra of m-methylaniline, J. Mol. Struct. (Theochem.) 625 (2003) 17–24.

[29] G. Varsanyi, Vibrational Spectra of Seven Hundred Benzene Derivatives, Adam Hilger, London, 1974.

[30] L.J. Bellamy, Infrared Spectra of Complex Molecules, Wiley, New York, 1959.

[31] V. Balachandran, V. Karunakaran, Quantum mechanical study of the structure and vibrational spectroscopic (FT-IR and FT-Raman), first-order hyperpolarizability, NBO and HOMO–LUMO studies of 4-bromo-3-nitroanisole, Spectrochim. Acta Part A 106 (2013) 284–298.

[32] Y. Yang, W. Zhang, X. Gao, Blue-shifted and red-shifted hydrogen bonds: theoretical study of the CH3CHO–HNO complexes, Int. J. Quantum Chem. 106 (2006) 1199–1207.

[33] J. Chocholousova, V. Vladimir Spirko, P. Hobza, First local minimum of the formic acid dimer exhibits simultaneously red-shifted O–H O and improper blue-shifted C–H O hydrogen bonds, Phys. Chem. Chem. Phys. 6 (2004) 37–41.

[34] R.S. Mulliken, Electronic population analysis on LCAO-MO molecular wave functions, J. Chem. Phys. 23 (1955) 1833–1840.

[35] J.S. Murray, K. Sen, Molecular Electrostatic Potentials, Concepts and Applications, Elsevier, Amsterdam, 1996.

[36] L. Zhang, Lu Ym, X.Y. Dong, Effects and mechanism of the selective COX-2 inhibitor, celecoxib, on rat colitis induced by trinitrobenzene sulfonic acid, China. j.dig. Dis. 5 (2004) 110–114.

[37] L.J. Marnett, Mechanisms of cyclooxygenase-2 inhibition and cardiovascular side effects: the plot thickens, Cancer Prev. Res. (Phila Pa) 2 (2009) 288–290.

[38] Y. Atalay, D. Avci, A. Basoglu, Linear and non-linear optical properties of some donor–acceptor oxadiazoles by ab initio Hartree-Fock calculations, Struct. Chem. 19 (2008) 239–246.

[39] T. Vijayakumar, I. Hubert Joe, C.P.R. Nair, V.S. Jayakumar, Efficient π electrons delocalization in prospective push–pull non-linear optical chromophore 4-[N,N-dimethylamino]-4'-nitrostilbene (DANS): a vibrational spectroscopic study, Chem. Phys. 343 (2008) 83–99.

[40] I. Fleming, Frontier Orbitals: Organic Chemical Reactions, Wiley, London, 1976.

[41] G. Gece, The use of quantum chemical methods in corrosion inhibitor studies, Corros. Sci. 50 (2008) 2981–2992.

[42] K. Fukui, Theory of Orientation and Stereo Selection, Springer–Verlag, Berlin, 1975.

[43] D.F.V. Lewis, C. Loannides, D.V. Parke, Interaction of a series of nitriles with the alcohol-inducible isoform of P450: computer analysis of structure–activity relationships, Xenobiotica 24 (1994) 401–408.

[44] R.G. Parr, L. Szentpaly, S. Liu, Electrophilicity index, J. Am. Chem. Soc. 121 (1999) 1922–1924.

[45] P.K. Chattaraj, B. Maiti, U. Sarkar, Electrophilicity equalization principle, J. Phys. Chem. 107A (2003) 4973–4975.

[46] R.G. Parr, R.A. Donnelly, M. Levy, W.E. Palke, Electronegativity: the density functional viewpoint, J. Chem. Phys. 68 (1978) 3801–3807.

[47] R.G. Parr, R.G. Pearson, Absolute hardness: companion parameter to absolute electronegativity, J. Am. Chem. Soc. 105 (1983) 7512–7516.

[48] R.G. Parr, P.K. Chattraj, Principle of maximum hardness, J. Am. Chem. Soc. 113 (1991) 1854–1855.

[49] R. Parthasarathi, J. Padmanabhan, M. Elango, V. Subramanian, P. Chattaraj, Intermolecular reactivity through the generalized philicity concept, Chem. Phys. Lett. 394 (2004) 225–230.

[50] R. Parthasarathi, J. Padmanabhan, V. Subramanian, B. Maiti, P. Chattaraj, Toxicity analysis of 3 3' 4 4' 5- pentachlorobiphenyl through chemical reactivity and selectivity profiles, Curr. Sci. 86 (2004) 535–542.

[51] R. Parthasarathi, J. Padmanabhan, V. Subramanian, U. Sarkar, B. Maiti, P. Chattaraj, Toxicity analysis of benzidine through chemical reactivity and

selectivity profiles: a DFT approach, Int. Electron. J. Mol. Des. 2 (2003) 798—813.

[52] B. Semire, Density functional theory studies on electronic properties of thiophene S-oxides as aromatic dienophiles for reactivity prediction in Diels-Alder reactions, Pak. J. Sci. Ind. Res. 56A (2013) 14—18.

[53] B. Semire, O.A. Odunola, Theoretical study of nucleophilic behavior of 3,4-dioxa-4-thia-cyclopenta[A]pentalene using ab initio and DFT based reactivity descriptors, Int. J. Chem. Model. 4 (2011) 87—96.

[54] L.R. Domingo, M.J. Aurell, P. Perez, P. Conteras, Quantitative characterization of the local electrophilicity of organic molecules. Understanding the regioselectivity on Diels—Alder Reactions, J. Phys. Chem. 106A (2002) 6871—6875.

[55] F. De Proft, P. Geerlings, Conceptual and computational DFT in the study of

[56] V. Sathyanarayanamoorthi, V. Kannappan, K. Sukumaran, Studies on free energies of solution and its components of thiazole amine derivatives, J. Mol. Liq. 174 (2012) 112—116.

[57] J.S. Murray, K. Sen, Molecular Electrostatic Potentials, Elsevier, Amsterdam, 1996.

[58] R. Zhang, B. Dub, G. Sun, Y. Sun, Experimental and theoretical studies on o-, m- and p-chlorobenzylideneaminoantipyrines, Spectrochim. Acta Part A 75 (2010) 1115—1124.

[59] E. Scrocco, J. Tomasi, Advances in Quantum Chemistry, Academic Press, New York, 1978.

aromaticity, Chem. Rev. 101 (2001) 1451—1464.